Chemical Bath Deposition of MoS_2 Thin Films on Plastic Optical Fibre for Room-Temperature Hydrogen Sensing

Khairun Nafi' Khairul Kamel[1], Mohd Rashid Yusof Hamid[2], Abdul Hadi Ismail[3,4], Nurul Atiqah Izzati Md Ishak[5], Nor Azlinah Md Lazam[1], Boon Hong Ong[2], Mohd Hanif Yaacob[6] and Nor Akmar Mohd Yahya[7]*

[1]University Malaysia of Computer Science and Engineering, VSQ@PJ City Centre, Jln Utara, Section 14, 46200 Petaling Jaya, Selangor Darul Ehsan, Malaysia

[2]Nanotechnology and Catalysis Research Centre (NANOCAT), Institute for Advanced Studies (IAS), Universiti Malaya 50603 Kuala Lumpur, Malaysia

[3]Centre of Innovative Nanostructures & Nanodevices (COINN), Universiti Teknologi PETRONAS, 32610 Seri Iskandar, Perak Darul Ridzuan, Malaysia

[4]Faculty of Data Science and Computing, Universiti Malaysia Kelantan City Campus, Pengkalan Chepa, 16100, Kota Bharu, Kelantan, Malaysia

[5]Carbon Dioxide Capture and Utilisation (CCDCU), Faculty of Engineering and Technology, Sunway University, No. 5 Jalan Universiti, Bandar Sunway, 47500 Petaling Jaya, Selangor Darul Ehsan, Malaysia

[6]Wireless and Photonics Network Research Centre, Faculty of Engineering, University Putra Malaysia, 43000 UPM Serdang, Selangor, Malaysia

[7]School of Engineering, Faculty of Engineering and Technology, Sunway University, No. 5, Jalan Universiti, Bandar Sunway, 47500 Selangor Darul Ehsan, Malaysia

*Corresponding author (e-mail: akmarm@sunway.edu.my)

Hydrogen gas (H_2) is an increasingly vital energy carrier, but its highly flammable nature demands reliable and selective sensing systems. In this study, an optical H_2 sensor was developed by coating two-dimensional molybdenum disulfide (MoS_2) thin films onto a side-polished plastic optical fibre (POF). The MoS_2 sensing layer was synthesized using the chemical bath deposition (CBD) method, producing nanostructured films with porous morphology (10–40 nm nanogranules) and good crystallinity as confirmed by XRD. The deposited MoS_2 layer adhered uniformly to the fibre surface, enabling strong interaction with the guided light through the exposed fibre core. Optical absorbance measurements revealed a clear, consistent response to H_2 concentrations (0.25–1.00 %), with a linear sensitivity of 0.3084 a.u./% H_2 (R^2 = 0.9476). The sensor exhibited rapid response times decreasing from 5 min at 0.25 % H_2 to 3 min at 1.00 % H_2, and recovery times between 5–7 min depending on concentration. These results confirm that nanostructured, crystalline MoS_2 coatings provide abundant active sites for H_2 adsorption, leading to fast and sensitive optical detection. This integration of CBD-grown MoS_2 with optical fibres demonstrates a promising pathway for low-power, electromagnetic interference (EMI) immune, and compact H_2 sensing applications.

Keywords: MoS_2, hydrogen sensor, optical fibre, optical sensing, chemical bath deposition, room-temperature

Received: September 2025; Accepted: February 2026

H_2 is increasingly regarded as a clean and sustainable energy vector due to its high energy density, non-toxic nature, and zero carbon emissions when employed in fuel cells [1, 2]. It plays a pivotal role in diverse industrial processes such as petroleum refining, ammonia synthesis, and methanol production [3, 4]. With growing momentum toward global decarbonization, H_2 is expected to support future low-carbon energy systems through grid stabilization, long-duration storage, and fuel for transportation infrastructure [5, 6].

Nevertheless, the physical properties of H_2 present significant safety concerns. As the lightest and smallest molecule, it can easily permeate through tiny gaps and rapidly diffuse into air [7]. Additionally, H_2 is colourless, odourless, and tasteless, making it difficult to detect without specialized sensors [5]. Its flammability range is broad (4-75 % by volume in air), and due to its low ignition energy, even small leaks can lead to catastrophic explosions if exposed to a spark or flame [8]. This makes the accurate detection of H_2 at low concentrations vital for safety in H_2 production, storage, and delivery [9].

Traditional H_2 sensors based on metal oxide semiconductors (MOS) exhibit high sensitivity and long-term stability; however, they typically require a

high operating temperature (200-400 °C), which increases energy consumption and limits safe deployment near flammable gases [10, 11]. Tang et al. reported a graphene-based H_2 sensor operating at room temperature, where UV-assisted carrier modulation and polymer molecular sieves enabled fast response (around 3s at 5 ppm) and improved humidity resistance; however, the sensing mechanism relied on electrical readouts and complex surface modification [12]. Other materials like conducting polymers offer room-temperature operation but suffer from poor repeatability and are sensitive to humidity, limiting their reliability in practical applications [9, 13].

To overcome these limitations, two-dimensional (2D) materials such as molybdenum disulfide (MoS_2) have gained attention for gas sensing applications due to their large surface-to-volume ratio, chemically active sites, and unique electronic structure [12, 14]. MoS_2, especially in its semiconducting 2H phase, allows gas adsorption that alters its optical and electronic properties, making it highly suitable for optical detection [15, 16]. However, achieving uniform and low-temperature deposition of MoS_2 on curved or flexible surfaces remains a fabrication challenge.

Optical fibre-based sensing platforms offer several advantages for H_2 detection, particularly in environments where electromagnetic interference (EMI), flammability, or remote access are concerns. These sensors are passive, intrinsically safe, and immune to EMI, making them ideal for harsh or hazardous environments. Luong et al. reported an optical H_2 sensor based on Pd and Pd-alloy nano-hydride, where H_2 absorption induced measurable changes in optical transmission, achieving sub-second response times and ppm-level detection limits at room temperature, while maintaining intrinsic electrical safety [17].

In another optical approach, Pd-based thin films and nanostructures integrated with optical transducers were tested for H_2 sensing, relying on H_2-induced modulation of optical intensity or wavelength shift, offering remote and EMI-immune detection but often involving complex material fabrication or noble-metal coatings [18]. Side-polished POF enables evanescent field interaction with the surrounding medium, making them suitable for integration with functional layers like MoS_2 for optical sensing [13, 19].

In this study, MoS_2 thin films were deposited onto side-polished POF using chemical bath deposition (CBD), a simple and cost-effective technique well suited for optical transducer fabrication [20, 21, 22, 23]. The fabricated MoS_2 coated POF was tested for its optical absorbance response to varying H_2 concentrations at room temperature, to confirm its functionality as a H_2 sensor. This work investigated the feasibility of employing MoS_2 thin films as an active sensing layer on optical fibres to obtain insights into the underlying sensing mechanism that enables low-power, EMI-immune, and highly sensitive H_2 detection.

EXPERIMENTAL

Materials

The materials used in this study included sodium sulphide (Na_2S, LabServ, 96.33-97.31 % purity), sulfuric acid (H_2SO_4, Merck, 95-97 % purity), and ammonium heptamolybdate ($(NH_4)_6Mo_7O_{24}$, Sigma-Aldrich, Assay 81.0-83.0 % purity).

Stage 1: Preparation of POF

POF with a core diameter of 1.0 mm and polymethyl methacrylate (PMMA) cladding were used as the optical substrate. A side-polishing process was conducted to expose the fibre core, enabling evanescent wave interaction with the sensing material, as shown in Figure 1. The cladding was partially removed over a 1.5 cm length using fine-grade sandpaper under controlled pressure to avoid damaging the core. The exposed section was cleaned using ethanol and dried at room temperature prior to coating.

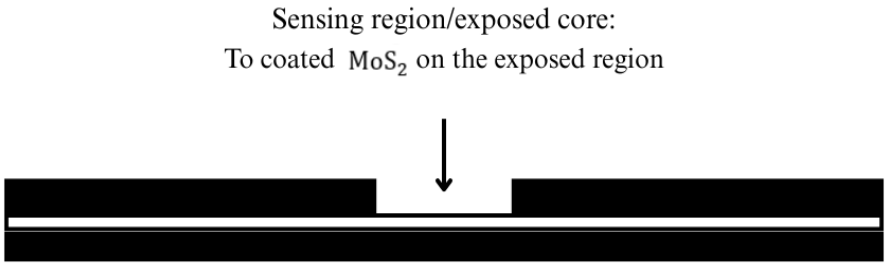

Figure 1. Illustration of side polished POF with exposed core for the evanescent wave interaction.

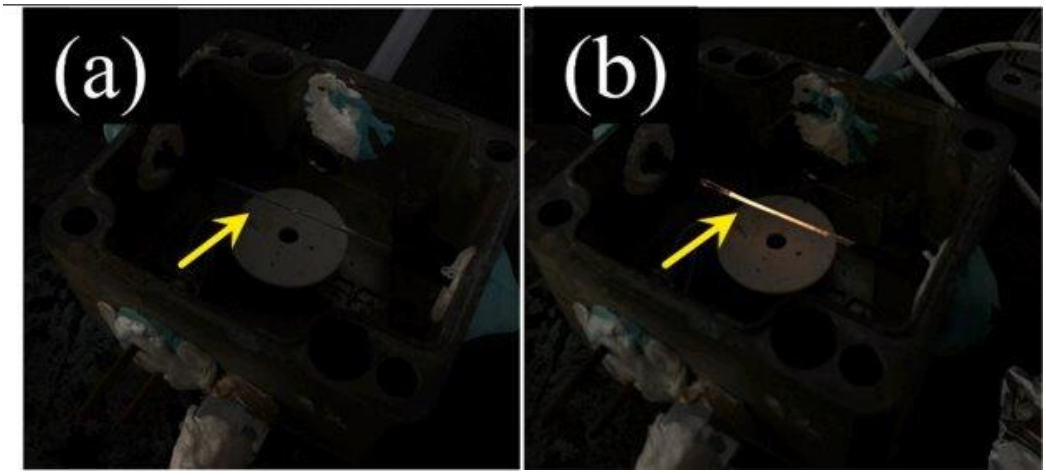

Figure 2. Photographic comparison of light propagation in POF: (a) cladded POF and (b) uncladded POF after side-polishing, both positioned inside the gas chamber.

To validate the effectiveness of the side-polishing process, Figure 2 presents photographic evidence of light propagation within the POF positioned inside the gas chamber. Figure 2(a) shows normal POF without any modification, where light confinement within the core is maintained due to total internal reflection. In contrast, Figure 2(b) shows the POF after side-polishing, wherein partial removal of the cladding exposed the core, allowing evanescent field leakage and enabling interaction with the external medium.

This comparison shows the difference in light propagation within the core and the leaking in cladding.

Stage 2: Synthesis of MoS_2

Molybdenum disulfide (MoS_2) thin films were deposited using a chemical bath approach, which leverages the in-situ generation of sulphide species and their subsequent complexation with molybdenum precursors. Initially, 10 mL of sodium sulphide (Na_2S, 0.2 M) was acidified with 1 mL of sulfuric acid (H_2SO_4, 1 M) in a fume hood, resulting in a turbid suspension attributed to the evolution of H_2S gas. The introduction of 10 mL ammonium heptamolybdate ($(NH_4)_6Mo_7O_{24}$, 1 mM) facilitated the formation of soluble thiomolybdate intermediates (e.g., MoS_4^{-2}), as evidenced by the dark orange/brown solution. The reaction bath was maintained at 60 °C to enhance precursor reactivity and drive subsequent reduction-sulfurization pathways toward MoS_2 nucleation.

The POF substrates were side-polished and subsequently pre-cleaned with ethanol prior to MoS_2 deposition. Then, the substrates were vertically immersed in the bath, where heterogeneous nucleation and oriented growth of MoS_2 nanosheets occurred over 30 min. Upon completion, the substrates were withdrawn, rinsed with deionized water to eliminate unreacted ionic species, and dried overnight under ambient conditions, yielding adherent MoS_2 coatings suitable for optical sensing applications.

The synthesis began with the acidification of sodium sulfide (Na_2S) using sulfuric acid (H_2SO_4), which generated hydrogen sulfide gas (H_2S) while leaving sodium sulfate (Na_2SO_4) in the aqueous phase (Equation 1). The freshly formed H_2S subsequently reacted under acidic conditions with molybdate species to promote sulfidation, producing the orange/brown tetrathiomolybdate ($Mo-S$) complex (Equation 2). This intermediate was essential, as its thermal decomposition in the final step yielded the targeted molybdenum sulfide product (Equation 3).

$$Na_2S(aq) + H_2SO_4(aq) \rightarrow H_2S(g) + Na_2SO_4\,(aq) \quad (1)$$

$$(NH_4)_6Mo_7O_{24} + 28H_2S \rightarrow 7(NH_4)_2MoS_4 + 24H_2O \quad (2)$$

$$(NH_4)_2MoS_4 \xrightarrow{\Delta} MoS_2(s) + 2NH_3(g) + H_2S\,(g) + S\,(s) \quad (3)$$

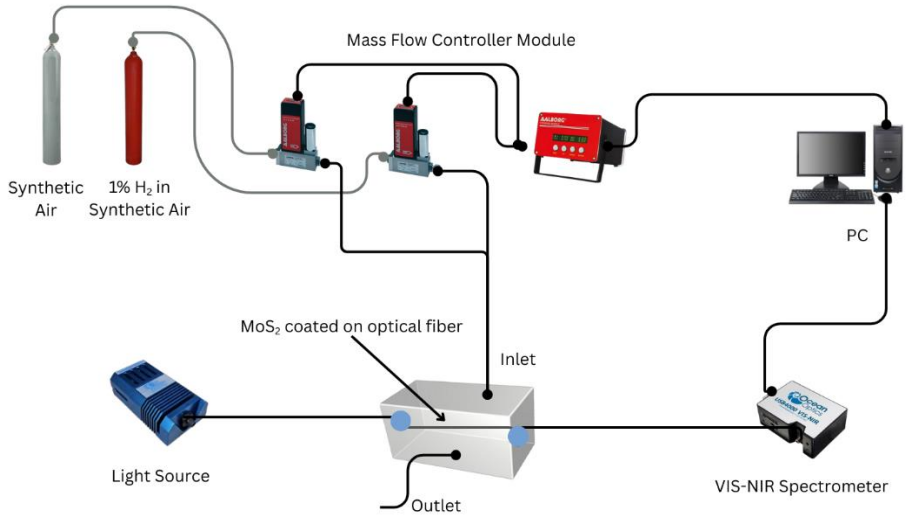

Figure 3. Schematic diagram of the optical H_2 sensing setup.

Stage 3: Optical Characterization Towards H_2

The POF coated with MoS_2 was placed inside a custom-built sealed gas chamber for sensing evaluation. A halogen light source was connected to one end of the fibre, and a spectrometer was attached to the other end to record transmitted light intensity. Optical absorbance was monitored in real time while the POF was exposed to H_2 gas at concentrations of 0.25 %, 0.5 %, 0.75 %, and 1.00 % in synthetic air. Each exposure cycle was followed by a recovery phase in synthetic air to evaluate sensor performance.

The sensing setup utilized the MoS_2-coated POF as the sensing element, as shown in Figure 3. The system included a halogen light source, sealed gas chamber, synthetic air and H_2 inputs via mass flow controllers, as well as a VIS–NIR spectrometer for real-time absorbance monitoring.

RESULTS AND DISCUSSION

Material Characterization

FESEM

Figure 4 shows FESEM micrographs of two different surface regions in the same MoS_2 coated sample at 100k× magnification. Both regions exhibited a porous and non-uniform network with interconnected voids, but with local variations in surface roughness and particle distribution. In Figure 4(a), the surface was dominated by smaller clusters of nanogranules (10 - 20 nm) decorating the pore walls. Meanwhile, figure 4(b) highlights the presence of larger agglomerates and a wider range of nanogranules, from 10 to 40 nm, forming over the porous framework. Such morphological heterogeneity is typical in solution-processed or deposited MoS_2 films and directly affects the density of active adsorption sites available for H_2 interactions. Similar porous and heterogeneous MoS_2 morphologies with nanoscale granules and interconnected voids have been widely reported, where variations in particle size, edge density, and surface roughness were found to strongly influence the availability of active sites for H_2-related surface reactions [24, 25].

Other observations have been reported in recent studies. Wu et al. observed that pristine MoS_2 displayed a flake-like porous structure, while Pd decoration introduced nanoparticles along the sheet edges and surfaces, modifying porosity and surface area [8]. Likewise, Ma et al. noted that Pd doping roughened the MoS_2 surface and introduced distinct grain boundaries compared to pristine films, which facilitated the creation of new adsorption sites for H_2 [26]. Kim et al. reported that noble metal nanoparticle decoration maintained the overall flake-like MoS_2 morphology while introducing uniformly distributed nanoclusters, thereby enhancing sensing activity through geometric and electronic effects [27].

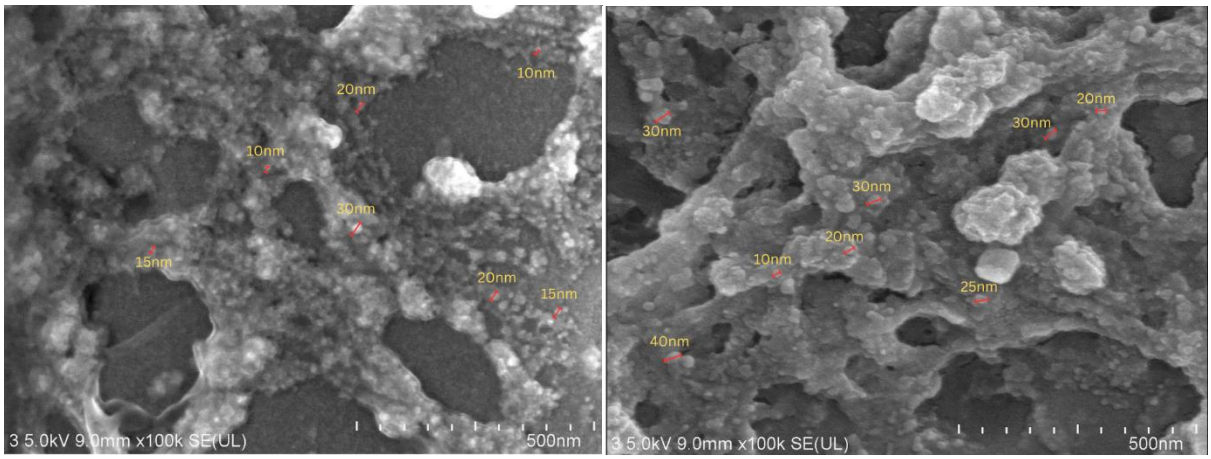

(a) (b)

Figure 4. FESEM micrographs of the MoS_2 coated sample at 100k times magnification showing different surface regions: (a) a porous surface with fine particle decoration along the pore walls; (b) a surface region with larger agglomerates distributed over the porous matrix.

To conclude, both images highlight the heterogeneous morphology of the same sample, which provided abundant active sites for H_2 adsorption.

EDS

EDS analysis was conducted to evaluate the elemental composition of the MoS_2 sensing layer. The spectra obtained from two different surface points of the sample revealed the dominant presence of molybdenum (Mo) and sulfur (S), confirming the successful formation of MoS_2 on the substrate. The atomic ratio between S and Mo at both points was consistent with the ideal stoichiometry of MoS_2, suggesting that the synthesis conditions were effective in promoting the targeted compound formation, in agreement with previous studies [8, 26].

In addition to Mo and S, carbon (C) and oxygen (O) were also detected. These elements are commonly attributed to adventitious carbon from environmental exposure or to residual organic species from precursor solutions used during the deposition process [27]. The detection of minor elements such as sodium (Na) and aluminum (Al) is likely due to contributions from the glass substrate, which may contain aluminosilicate or soda-lime components. Such occurrences are frequently observed in thin film studies involving glass-supported deposition [26].

Element	Weight %	Atomic %
C K	12.68	30.28
O K	12.18	21.84
Na K	2.64	3.30
Al K	0.94	1.00
S K	37.43	33.49
Mo L	32.81	9.81
Ba L	1.32	0.28
Total	100.00	

Figure 5. EDS elemental composition (weight% and atomic%) of the MoS_2-coated POF.

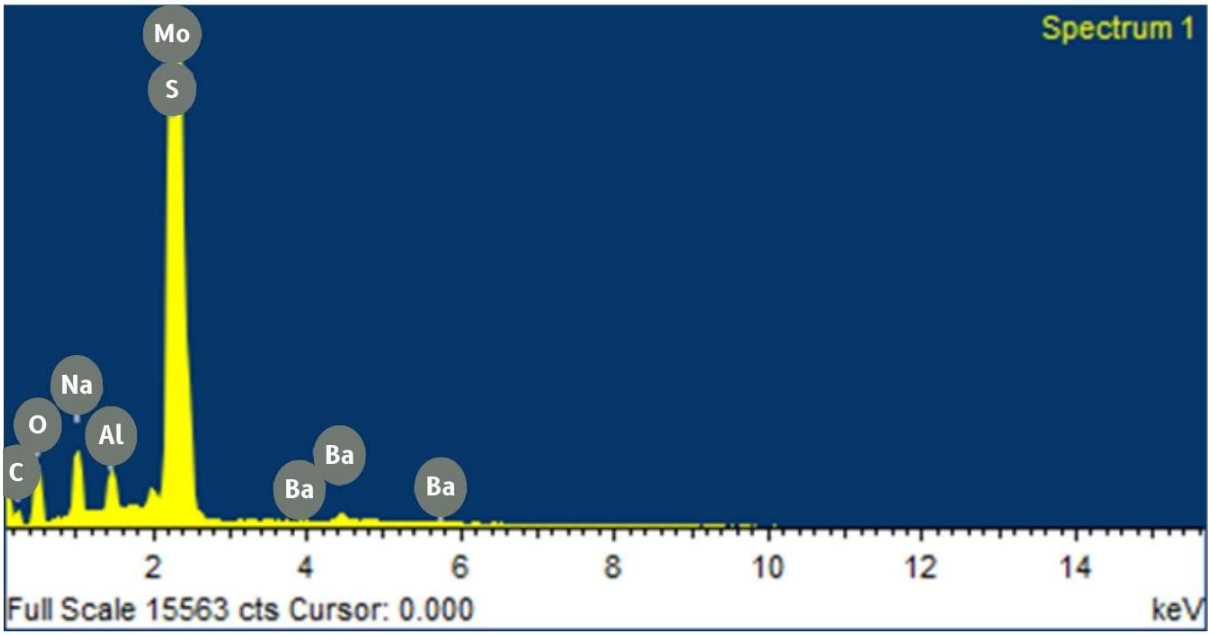

Figure 6. Energy-dispersive X-ray spectroscopy (EDS) spectrum of the synthesized MoS_2 film.

Furthermore, a low-intensity barium (Ba) signal was identified at both measurement points. This is presumed to originate from the underlying glass substrate, particularly if it contained barium-based constituents. Similar substrate-related Ba detection has been reported in EDS analyses where high accelerating voltages permit deeper X-ray interaction with the substrate material [8]. The minimal level of Ba observed was not expected to interfere with the chemical or sensing characteristics of the MoS_2 layer.

Overall, the EDS results confirmed the elemental composition and purity of the MoS_2 film, with no evidence of foreign contamination that would compromise the performance of the hydrogen sensor.

XRD

The XRD pattern of the synthesized MoS_2 nanostructures (Figure 7) showed distinct diffraction peaks at 2θ values of approximately 32.03°, 33.87°, 38.68°, 43.04°, and 48.76°. These peaks were indexed to the (100), (101), (103), (006), and (105) crystallographic planes of the hexagonal 2H-MoS_2 phase, in agreement with the JCPDS standard data. The presence of these well-defined peaks confirmed the successful formation of crystalline MoS_2 [28].

The relatively broad nature of the diffraction peaks indicates the nanostructured character of the material, which is often associated with a small crystallite size and lattice strain. The slight deviations in peak positions compared to standard reference values may arise from internal stress, size-induced broadening, or interfacial interactions with the underlying substrate during the deposition process [28].

The XRD analysis verified that the synthesized sample was predominantly crystalline MoS_2 with a hexagonal structure, and the observed broadening suggests that the material possessed nanoscale features favourable for gas-sensing applications due to the increased surface-to-volume ratio.

Sensor Performance

The n-type semiconductor nature of MoS_2 originates from the availability of sulfur vacancies, which not only release free electrons but also act as active adsorption sites for gas molecules. This trait makes MoS_2 highly responsive to changes in the chemical environment [29]. So, when MoS_2 is exposed to H_2 at room temperature, physical adsorption and electronic doping occur simultaneously. The dissociative adsorption of H_2 forms $S-H$ bonds on the MoS_2 surface, where H_2 atoms serve as electron donors, as in Equation 4. This increases the carrier concentration, which raises the Fermi level and enhances n-type conductivity [16].

$$H_2 \rightarrow 2H \rightarrow 2H^+ \rightarrow 2e^- \quad (4)$$

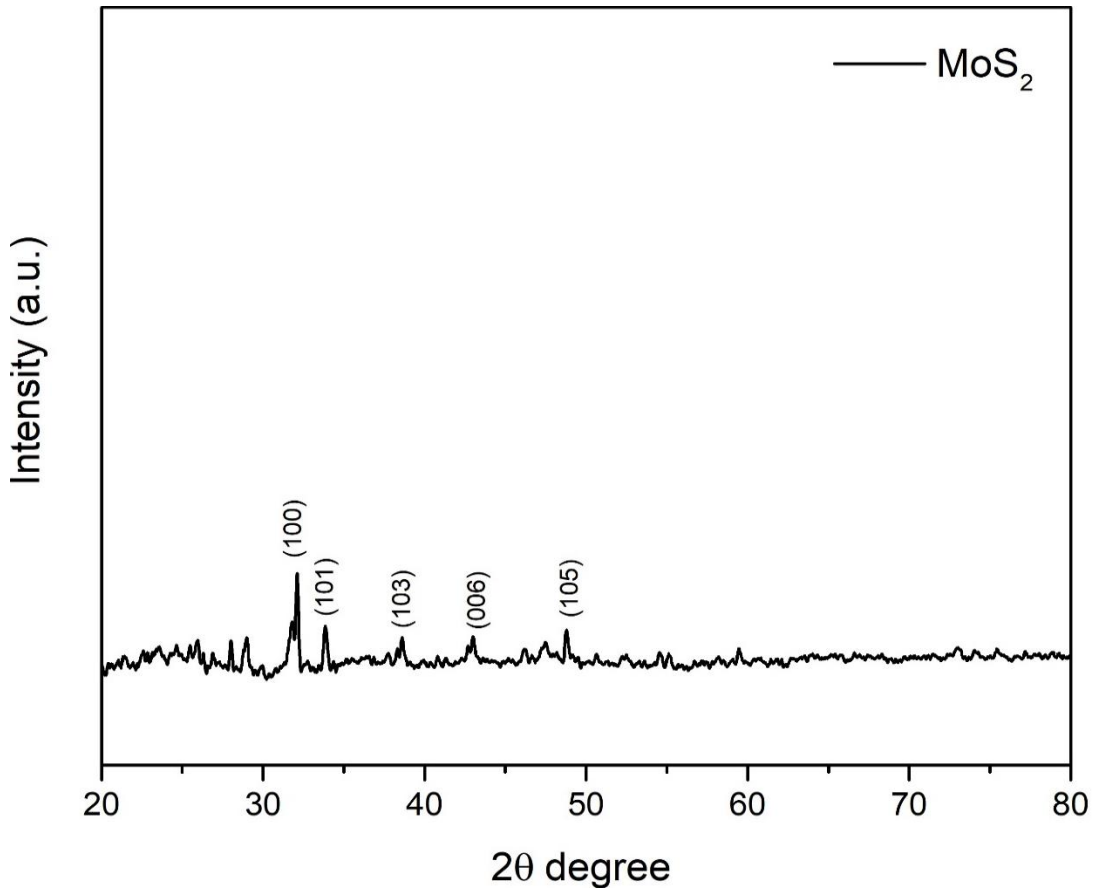

Figure 7. X-Ray diffractogram of the synthesized MoS_2.

These electrons enter the conduction band of MoS_2, modifying its dielectric function [30]. However, no formal redox reaction takes place at this stage. Molybdenum remains in the Mo^{+4} oxidation state as the electron donation only happens at the surface. Instead of permanent chemical conversion, H_2 molecules go through physical adsorption at sulfur vacancies or catalytic sites, where they donate electrons to the MoS_2 lattice. Nevertheless, this process still modulates the electronic states and optical absorption of MoS_2, providing a stable platform for sensing under ambient conditions [15].

These hydrogen-induced variations in the optical properties of MoS_2 can be effectively monitored through absorbance measurements. In optical fibre-based sensor configurations, the evanescent field generated by total internal reflection (TIR) interacts with the MoS_2 layer deposited on the exposed fibre region. Any adsorption-induced modulation in MoS_2 electronic states alter its absorbance, and these variations can be directly captured by the optical fibre transducer [30]. Generally, the optical characteristics are governed by the complex refractive index, $\bar{n}$, in Equation 5.

$$\bar{n} = n + ik \tag{5}$$

Here, n denotes the real part, governing the phase velocity of light, and k is the extinction coefficient, associated with absorption. Upon H_2 exposure, both n and k increase due to enhanced free-carrier interactions. This results in stronger light–matter coupling and higher optical losses. The absorption coefficient α is related to k as in Equation 6.

$$\alpha = \frac{4\pi k}{\lambda} \tag{6}$$

When the extinction coefficient, k, increases due to H_2 exposure, α also increases [31]. This means that more of the incident light is attenuated by the MoS_2 film due to the increased absorption coefficient. Equation 7 displays the relation between absorbance, A, with the absorption coefficient, α.

$$A = \log_{10}\frac{I_0}{I} = \alpha d \tag{7}$$

where I_0 is the incident light intensity, I is the transmitted light intensity and d is the thickness of the absorbing layer. As α increases due to H_2 exposure, absorbance increases proportionally [32]. This could be observed as a higher absorbance peak in spectroscopic measurements.

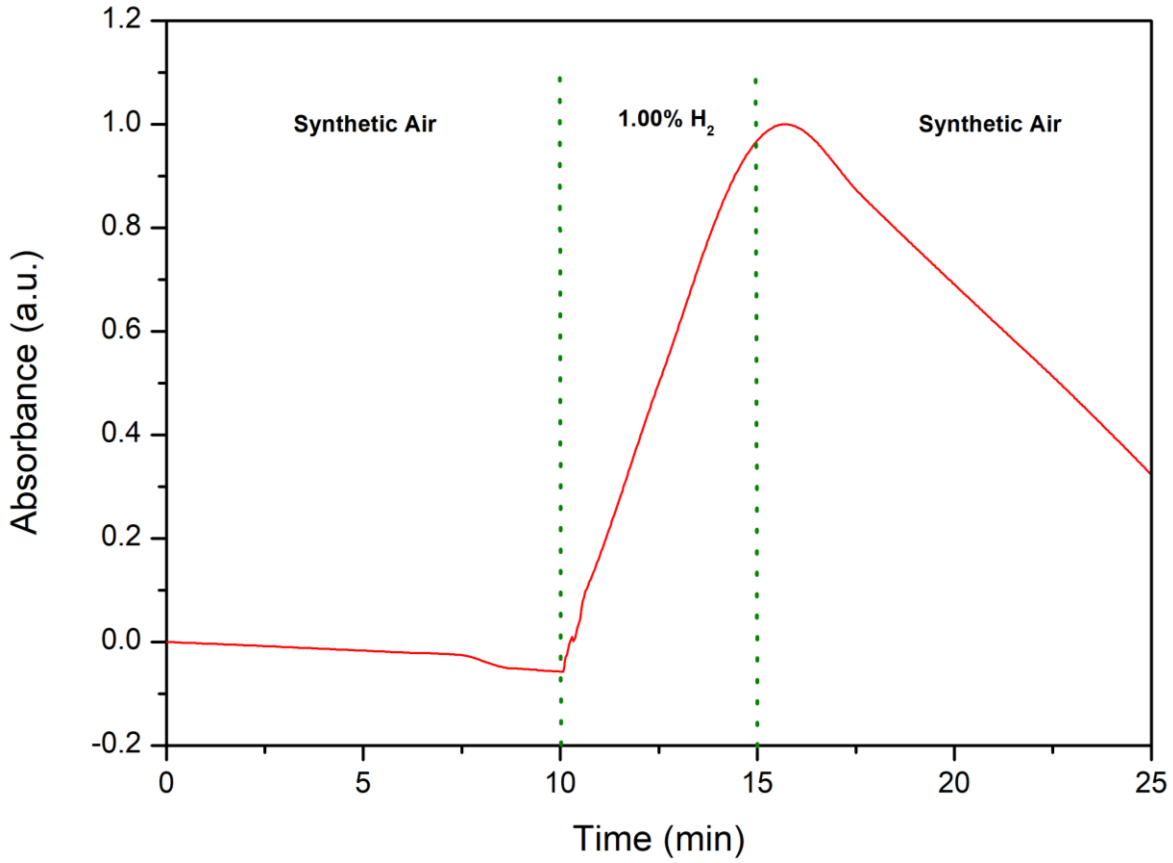

Figure 8. Dynamic optical absorbance response of the MoS_2 coated POF under cyclic exposure to 1.00 % H_2 and synthetic air.

The corresponding graph is presented in Figure 8, which illustrates the MoS_2 coated fibre under 100 % synthetic air and 1 % H_2 exposure.

Under H_2 exposure, MoS_2 surfaces exhibited enhanced absorbance due to electron donation from dissociated H_2 molecules. These electrons increased the free-carrier concentration, which modified the refractive index and strengthened optical absorption. Conversely, when the environment was switched back to synthetic air (a mixture of N_2 and O_2), the absorbance decreased toward its baseline level. This recovery indicates that once the H_2 exposure was removed, the sensor response gradually returned to its baseline level, demonstrating stable and repeatable performance under ambient conditions.

The absorbance profile in Figure 9 illustrates the sensor response over multiple exposure–recovery cycles. During each cycle, H_2 was introduced after baseline stabilization in synthetic air. An increase in absorbance followed by partial recovery was observed. The response pattern was repeatable but demonstrated a cumulative adsorption effect, suggesting incomplete H_2 desorption. This effect became more prominent in subsequent cycles, confirming strong $MoS_2 - H_2$ surface interactions.

Recovery Limitations and Proposed Improvement Strategies

To address the observed cumulative adsorption and incomplete recovery behaviour, one promising approach is the development of MoS_2-based composite sensing layers. The incorporation of secondary materials, such as noble metal catalysts or metal oxides, modifies the local electronic structure and facilitates charge redistribution. Pt-decorated MoS_2 has been shown to enhance H_2 dissociation and promote efficient carrier transfer across the MoS_2/ Pt interface, resulting in improved reversibility [33].

Similarly, MoS_2/WO_3 composite systems form heterojunctions with favourable band alignments, where charge transfer improves adsorption–desorption balance and recovery behaviour compared to pristine MoS_2. These studies indicate that heterointerface-induced charge redistribution weakens excessively strong gas–surface binding and enhances reversibility during repeated sensing cycles [34].

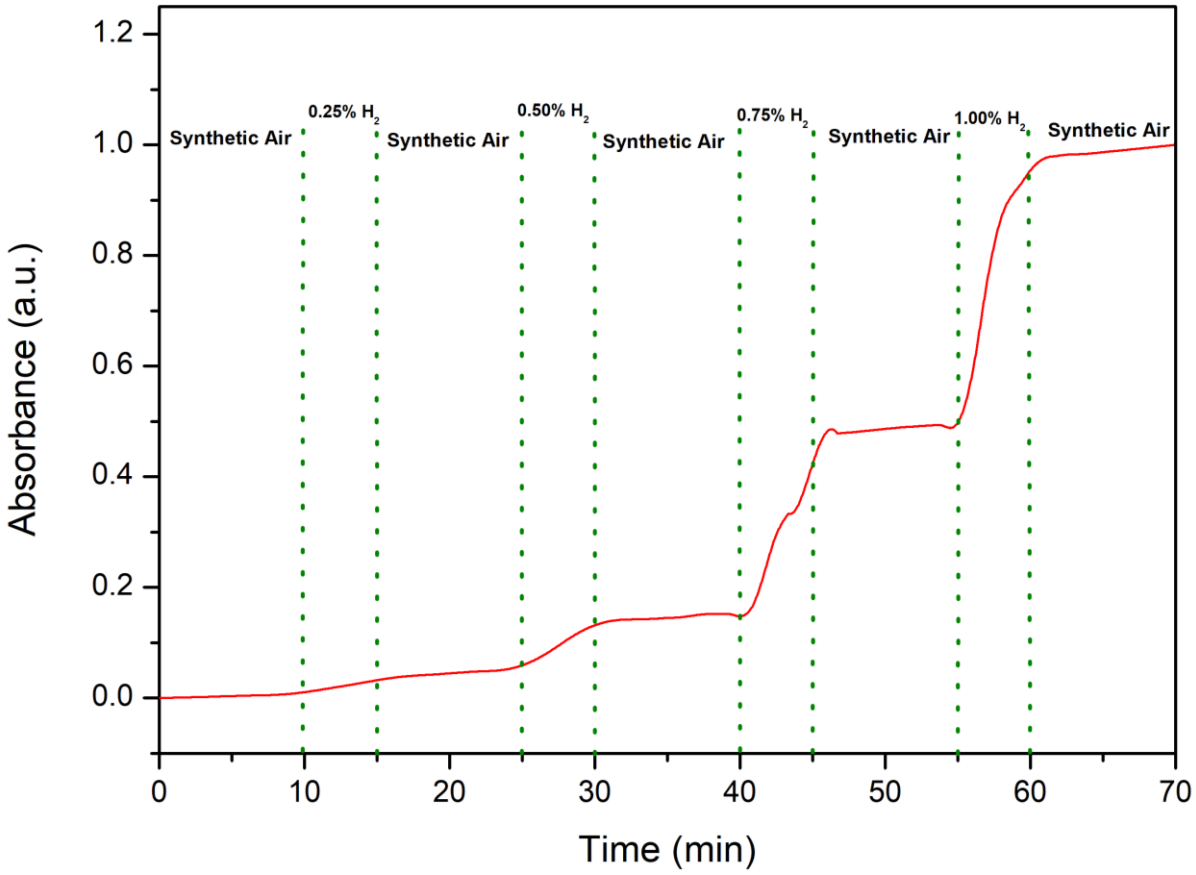

Figure 9. The dynamic optical response of the sensor over full synthetic air-H_2-air cycles.

In addition to material modification, post-deposition annealing treatment represents an effective strategy to improve recovery behaviour. Thermal annealing has been widely reported to remove residual solvents and surface-adsorbed water, reduce defect-related trap states, and improve crystallinity, thereby promoting faster and more reversible adsorption processes in semiconductor-based gas sensors [35].

Accordingly, future work will focus on MoS_2-based nanocomposite integration and optimization of post-deposition annealing conditions to mitigate cumulative adsorption effects while preserving the advantages of room-temperature, optical, and fibre-based H_2 sensing.

Figure 10 shows the cumulative absorbance variation of the sensor as a function of H_2 concentration in pure synthetic air: 0.25 % (2500 ppm), 0.5 % (5000 ppm), 0.75 % (7500 ppm), and 1.0 % (10000 ppm). A clear linear relationship was observed, as described by the regression equation $y = 0.3084x + 0.0017$ with a correlation coefficient $R^2 = 0.9476$. The slope of the calibration curve indicated an optical sensitivity of 0.3084a.u./% H_2, demonstrating that the sensor quantitatively detected H_2 concentrations within the tested range with good linearity.

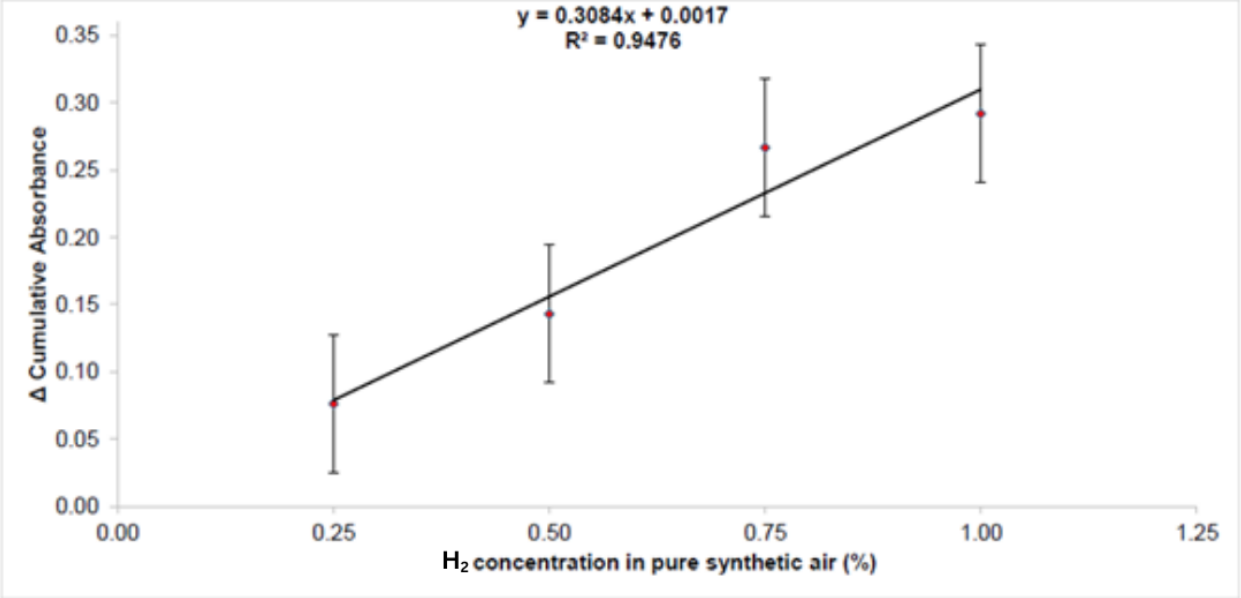

Figure 10. Cumulative absorbance changes vs H_2 concentration.

CONCLUSION

In this study, an optical H_2 sensor was successfully developed by integrating chemically synthesized MoS_2 thin films with a side-polished POF. The MoS_2 coating was deposited using a simple and low-temperature CBD process.

The sensor demonstrated a clear increase in optical absorbance upon exposure to H_2, with a linear relationship between absorbance and H_2 concentration in the range of 0.25 - 1.00 %. The optical sensitivity was determined to be 0.3084 a.u./% H_2 with a strong linearity (R^2 = 0.9476), indicating reliable quantitative detection across the tested concentration range. Dynamic optical response revealed repeatable sensor responses across multiple exposure and recovery cycles, though with partial recovery due to cumulative adsorption effects. It was observed that at 0.25 % H_2 concentration, the cumulative absorbance increased by 0.0217 a.u. In contrast, at 1 % H_2, the cumulative absorbance showed a much larger increase of 0.4558 a.u. This indicates that higher H_2 concentrations resulted in a stronger absorbance response.

Material characterization confirmed the successful formation of crystalline MoS_2 with appropriate morphology and composition. The sensing mechanism was attributed to surface adsorption of H_2 molecules, electron donation to the MoS_2 layer, and resulting changes in its electronic and optical properties.

This work demonstrates the potential of using MoS_2 coated optical fibres for compact, low-power, and EMI-immune H_2 sensing platforms. Further improvements in recovery behaviour and selectivity may pave the way for real-time monitoring applications in H_2 energy systems and industrial safety settings.

ACKNOWLEDGEMENTS

This research was funded by the Ministry of Higher Education, Malaysia and University Malaysia of Computer Science and Engineering, under grant number FRGS/1/2023/TK07/UNIMY/02/1, and by the Research Accelerator Grant Scheme (RAGS) from Sunway University, grant number GRTIN-RAG-DEN-08-2024.

REFERENCES

1. Younas, M., Shafique, S., Hafeez, A., Javed, F. and Rehman, F. (2022) An Overview of Hydrogen Production: Current Status, Potential, and Challenges. *Fuel*, **316**, 123317. doi: 10.1016/J.FUEL.2022.123317.

2. Cho, U. J., Jang, D., Jeon, Y., Kim, T., Jo, B., Kim, R., Kim, Y. and Kwon, M.-W. (2003) A Palladium-Deposited Molybdenum Disulfide-Based Hydrogen Sensor at Room Temperature. *Applied Sciences*, **13(19)**, 10594. doi: 10.3390/app131910594.

3. Nnabuife, S. G., Ugbeh-Johnson, J., Okeke, N. E. and Ogbonnaya, C. (2022) Present and Projected Developments in Hydrogen Production: A Technological Review∗. *Carbon Capture Science*

& Technology, **3**, 100042. doi: 10.1016/ J.CCST.2022.100042.

4. Atsbha, T. A., Yoon, T., Seongho, P. and Lee, C. J. (2021) A review on the catalytic conversion of CO2 using H2 for synthesis of CO, methanol, and hydrocarbons. *Journal of CO2 Utilization*, **44**, 101413. doi: 10.1016/J.JCOU.2020. 101413.

5. Alaghmandfard, A., Fardindoost, S., Frencken, A. L. and Hoorfar, M. (2024) The next generation of hydrogen gas sensors based on transition metal dichalcogenide-metal oxide semiconductor hybrid structures. *Elsevier Ltd*.. doi: 10. 1016/ j.ceramint.2024.05.259.

6. Amin, M., Butt, A. S., Ahmad, J., Lee, C., Azam, S. U., Mannan, H. A., Naveed, A. B., Farooqi, Z. U. R., Chung, E. and Iqbal, A. (2023) Issues and challenges in hydrogen separation technologies. *Energy Reports*, **9**, 894–911. doi: 10.1016/ J.EGYR. 2022. 12.014.

7. Jung, J. K., Kim, I. G., Chung, K. S., Il Kim, Y. and Kim, D. H. (2021) Determination of permeation properties of hydrogen gas in sealing rubbers using thermal desorption analysis gas chromatography. *Sci. Rep.*, **11**, 1. doi: 10.1038/s41598-021-96266-y.

8. Wu, H., Zhang, W., Yuan, H., Lin, G., Xie, H. and Jiang, T. (2025) Enhanced H2 sensing performance of Pd decorated MoS2: Experimental and DFT Insights. *J. Alloys Compd*, **1010**. doi: 10.1016/j.jallcom.2024.178139.

9. Verma, G., Venkatesan, P., Barala, S., Kumar, M., Dega, N. K. and Gupta, A. (2025) Hierarchical MoS2 Nanostructured Tubes on Biodegradable and Flexible Chitosan-Based Platform for Low-Temperature Hydrogen Detection. *IEEE Sens. J.*, **25(7)**, 11868–11875. doi: 10.1109/JSEN. 2025.3538705.

10. Ou, L. X., Liu, M. Y., Zhu, L. Y., Zhang, D. W. and Lu, H. L. (2022) Recent Progress on Flexible Room-Temperature Gas Sensors Based on Metal Oxide Semiconductor. *Springer Science and Business Media B.V.* doi: 10.1007/s40820-022-00956-9.

11. Zhu, L. Y., Ou, L. X., Mao, L. W., Wu, X. Y., Liu, Y. P. and Lu, H. L. (2023) Advances in Noble Metal-Decorated Metal Oxide Nanomaterials for Chemiresistive Gas Sensors: Overview. *Springer Science and Business Media B.V.* doi: 10.1007/s40820-023-01047-z.

12. Tang, C., Jin, W., Xiao, X., Qi, X., Ma, Y. and Ma, L. (2025) Graphene-based chemiresistive hydrogen sensor for room temperature operation. *Sens. Actuators B. Chem.*, **424**, 136889. doi: 10.1016/J.SNB.2024.136889.

13. Yahya, N. A. M., Hamid, M. R. Y., Ong, B. H., Rahman, N. A., Mahdi, M. A. and Yaacob, M. H. (2020) H2 Gas Sensor Based on Pd/ZnO Nanostructures Deposited on Tapered Optical Fiber. *IEEE Sens. J.*, **20(6)**, 2982–2990. doi: 10.1109/JSEN.2019.2957838.

14. Abdulhameed, A. and Mahnashi, Y. (2023) Fabrication of carbon nanotube/titanium dioxide nanomaterials-based hydrogen sensor using novel two-stage dielectrophoresis process. *Mater. Sci. Semicond Process*, **167**, 107794. doi: 10.1016/J.MSSP.2023.107794.

15. Yang, S., Liu, Y., Lei, G., Xie, Y., Peng, L., Xu, H., Wang, Z. and Gu, H. (2021) A DFT study on the hydrogen storage performance of MoS2 mono-layers doped with group 8B transition metals. *Int. J. Hydrogen Energy*, **46**, 24233–24246. doi: 10.1016/j.ijhydene. 2021. 04.200.

16. Park, C. H., Koo, W. T., Lee, Y. J., Kim, Y. H., Lee, J., Jang, J. S., Yun, H., Kim, I. D. and Kim, B. J. (2020) Hydrogen Sensors Based on MoS2Hollow Architectures Assembled by Pickering Emulsion. *ACS Nano*, **14(8)**, 9652–9661. doi: 10.1021/acsnano.0c00821.

17. Luong, H. M., Pham, M. T., Guin, T., Pokharel Madhogaria, R., Phan, M.-H., Larsen, G. K. and Nguyen, T. D. (2021) Sub-second and ppm-level optical sensing of hydrogen using templated control of nano-hydride geometry and composition. *Nat. Commun.*, **12**. doi: 10.1038/ s41467-021-22697-w.

18. Chen, K., Yuan, D. and Zhao, Y. (2021) Review of optical hydrogen sensors based on metal hydrides: Recent developments and challenges. *Elsevier Ltd*. doi: 10.1016/j.optlastec.2020. 106808.

19. Zhuo, L., Tang, J., Zhu, W., Zheng, H., Guan, H., Lu, H., Chen, Y., Luo, Y., Zhang, J., Zhong, Y., Yu, J. and Chen, Z. (2023) Side Polished Fiber: A Versatile Platform for Compact Fiber Devices and Sensors. *Springer Verlag*, Mar. doi: 10.1007/s13320-022-0661-x.

20. Elzawiei, Y. S. M., Hashim, M. R., Abdulhameed, A. and Halim, M. M. (2025) The role of synthesizing time on the optoelectronic properties of TiO2-ZnO nanocomposite on PTFE substrate fabricated by the chemical bath deposition method. *Physica B. Condens Matter*, **697**, 416734. doi: 10.1016/J.PHYSB.2024.416734.

21. Chua, W. H., Yaacob, M. H., Tan, C. Y. and Ong, B. H. (2021) Chemical bath deposition of h-MoO3

on optical fibre as room-temperature ammonia gas sensor. *Ceram Int.*, **47(23)**, 32828–32836. doi: 10.1016/J.CERAMINT.2021.08.179.

22. Sengupta, S., Aggarwal, R. and Raula, M. (2023) A review on chemical bath deposition of metal chalcogenide thin films for heterojunction solar cells. *Springer Nature*. doi: 10.1557/ s43578-022-00539-9.

23. Abdulhameed, A., Mahnashi, Y., Absi, M. A. A. and Drmosh, Q. A. (2025) ZnO Nanorods Grown on PLA-CF Mesh as Nanostructure Capacitance-Based Dust Sensor. *IEEE Sens. J.*, **25(19)**, 35773–35781. doi: 10.1109/JSEN.2025.3598458.

24. Li, Y., Gu, Q., Johannessen, B., Zheng, Z., Li, C., Luo, Y., Zhang, Z., Zhang, Q., Fan, H., Luo, W., Liu, B., Dou, S. and Liu, H. (2021) Synergistic Pt doping, and phase conversion engineering in two-dimensional MoS2 for efficient hydrogen evolution. *Nano Energy*, **84**. doi: 10.1016/j.nanoen. 2021.105898.

25. Wang, H., Xiao, X., Liu, S., Chiang, C.-L., Kuai, X., Peng, C.-K., Lin, Y.-C., Meng, X., Zhao, J., Choi, J., Lin, Y.-G., Lee, J.-M. and Gao, L. (2019) Structural and Electronic Optimization of MoS2 Edges for Hydrogen Evolution. *J. Am Chem. Soc.*, **141(46)**, 18578–18584. doi: 10.1021/jacs.9b09932.

26. Ma, E., Xu, Z., Sun, A., Yang, S. and Jiang, J. (2025) High-Performance Hydrogen Gas Sensor Based on Pd-Doped MoS2/Si Heterojunction. *Sensors*, **25(15)**, 4753. doi: 10.3390/ s25154753.

27. Kim, T., Lee, T. H., Park, S. Y., Eom, T. H., Cho, I., Kim, Y., Kim, C., Lee, S. A., Choi, M.-J., Suh, J. M., Hwang, I.-S., Lee, D., Park, I. and Jang, H. W. (2023) Drastic Gas Sensing Selectivity in 2-Dimensional MoS2 Nanoflakes by Noble Metal Decoration. *ACS Nano*, **17(5)**, 4404–4413. doi: 10.1021/acsnano.2c09733.

28. Kumar, N., Siroha, P., Sharma, Y., Singh, D., Dey, K., Kumar, R., Borkar, H. and Gangwar, J. (2021) Probing on crystallographic structural and surface morphology of hydro-thermally synthesized MoS2 nanoflowers consisting of nanosheets. *Applied Surface Science Advances*, **6**. doi: 10.1016/j.apsadv.2021.100167.

29. Verma, G., Gokarna, A., Kadiri, H., Nomenyo, K., Lerondel, G. and Gupta, A. (2023) Multiplexed Gas Sensor: Fabrication Strategies, Recent Progress, and Challenges. *American Chemical Society*. doi: 10.1021/acssensors.3c01244.

30. Brissinger, D. (2024) Modeling the Impact of Dye Concentration on Polymer Optical Properties via the Complex Refractive Index: A Pathway to Optical Engineering. *Polymers (Basel)*, **16**. doi: 10.3390/polym16050660.

31. Liu, C. P., Foo, Y., Kamruzzaman, M., Ho, C. Y., Zapien, J. A., Zhu, W., Li, Y. J., Walukiewicz, W. and Yu, K. M. (2016) Effects of Free Carriers on the Optical Properties of Doped CdO for Full-Spectrum Photovoltaics. *Phys. Rev. Appl.*, **6**. doi: 10.1103/PhysRev Applied. 6.064018.

32. Mayerhöfer, T. G., Pahlow, S. and Popp, J. (2020) The Bouguer-Beer-Lambert Law: Shining Light on the Obscure. *NLM (Medline)*.doi: 10.1002/ cphc.202000464.

33. Lee, S., Kang, Y., Lee, J., Kim, J., Shin, J. W., Sim, S., Go, D., Jo, E., Kye, S., Kim, J. and An, J. (2022) Atomic layer deposited Pt nanoparticles on functionalized MoS2 as highly sensitive H2 sensor. *Appl. Surf. Sci.*, **571**, 151256. doi: 10.1016/J.APSUSC.2021.151256.

34. Singh, S. and Sharma, S. (2022) Temperature-Based Selective Detection of Hydrogen Sulfide and Ethanol with MoS2/WO3 Composite. *ACS Omega*, **7(7)**, 6075–6085. doi: 10.1021/ acsomega.1c06471.

35. Krishna, K. G., Parne, S., Pothukanuri, N., Kathirvelu, V., Gandi, S. and Joshi, D. (2022) Nanostructured metal oxide semiconductor-based gas sensors: A comprehensive review. *Sens Actuators A Phys*, **341**, 113578. doi: 10.1016/ J.SNA.2022.113578.